Organic Electronics 13 (2012) 1277–1288

Contents lists available at SciVerse ScienceDirect

Organic Electronics

journal homepage: www.elsevier.com/locate/orgel

Solution-processed blue–green organic light-emitting diodes based on cationic iridium complexes with 1-pyridyl-3-methylimidazolin-2-ylidene-C,$C^{2'}$ as the ancillary ligand

Fuli Zhang, Lian Duan *, Juan Qiao, Guifang Dong, Liduo Wang, Yong Qiu *

Key Lab of Organic Optoelectronics and Molecular Engineering of Ministry of Education, Department of Chemistry, Tsinghua University, Beijing 100084, PR China

ARTICLE INFO

Article history:
Received 15 February 2012
Received in revised form 8 March 2012
Accepted 18 March 2012
Available online 5 April 2012

Keywords:
Organic light-emitting diode
Solution process
Cationic iridium complex
Blue–green light emission

ABSTRACT

Two new blue emitting cationic iridium complexes with N-heterocyclic carbene–pyridine as the ancillary ligand, namely, $[Ir(ppy)_2(pymi)]PF_6$ and $[Ir(dfppy)_2(pymi)]PF_6$ (pymi is 1-pyridyl-3-methylimidazolin-2-ylidene-C,$C^{2'}$, ppy is 2-phenylpyridine, dfppy is 2-(2,4-difluorophenyl)pyridine and PF_6^- is hexafluorophosphate), have been prepared, and the photophysical and electrochemical properties together with X-ray crystal structures have been investigated. In CH_3CN solutions, $[Ir(ppy)_2(pymi)]PF_6$ and $[Ir(dfppy)_2(pymi)]PF_6$ exhibit blue light emission with the peaks at 472 and 451 nm, respectively. Both photophysical properties and quantum chemical calculations indicate that photoluminescences of these complexes are mainly from ppy- or dfppy-based $^3\pi \rightarrow \pi^*$ states. Solution-processed organic light-emitting diodes (OLEDs) based on $[Ir(ppy)_2(pymi)]PF_6$ and $[Ir(dfppy)_2(pymi)]PF_6$ give blue–green electroluminescence (506 and 482 nm, respectively). At a doping concentration of 5 wt.%, the device based on $[Ir(ppy)_2(pymi)]PF_6$ reaches a maximum efficiency of 5.2 cd A^{-1}, which indicates that this complex is a promising phosphor for achieving efficient electrophosphorescence in the blue–green region.

1. Introduction

In the past two-plus decades, organic light emitting diodes (OLEDs) have received great attention for their application in flat panel display (FPD) and solid state lighting (SSL) as they offer several advantages for self-emitting displays, a wide viewing angle (almost 180°), a thin panel (<2 mm), light weight, a fast response time (microseconds and less), high contrast, flexible display, bright emission and surface emitting [1–9]. Compared with other components in OLEDs, e.g., electrodes, electron/hole transports, hosts, light emitting materials are considered to be the core of OLEDs [10], because their photophysical properties have a direct impact on the performance of OLEDs. Since influential and pioneering work made by Forrest et al. [11], heavy transition metal complexes have been attracting increasing attention due to their harvesting both singlet and triplet excitons for phosphorescence emission to present internal quantum efficiency of 100% in OLED [12–15], which are superior to fluorescent emitters, for which only singlet excitons can be harvested, giving an upper efficiency limit of 25%. Compared with other transition metal complexes [16–27], iridium(III) complexes are interesting candidates for OLEDs owing to their short excited-state lifetimes, high photoluminescence quantum yields and pronounced ligand-field-splitting effects of the trivalent iridium ion.

Currently, among the three primary RGB colors, red and green phosphorescent materials have been or are being commercialized, respectively [10,28,29]. However, the development of highly efficient and long-term stable blue phosphors and corresponding devices is still an ultimate challenge to commercialization of full color displays and white light resources. In 2001, Thompson et al. first

* Corresponding authors. Tel.: +86 10 62779988; fax: +86 10 62795137.
E-mail addresses: duanl@mail.tsinghua.edu.cn (L. Duan), qiuy@mail.tsinghua.edu.cn (Y. Qiu).

1566-1199/$ - see front matter © 2012 Elsevier B.V. All rights reserved.
http://dx.doi.org/10.1016/j.orgel.2012.03.017

demonstrated high-efficiency sky-blue OLEDs based on phosphorescent dopant Firpic [30]. Ever since then, some endeavors were made to search for better blue phosphors by modifying the ancillary chelate of FIrpic, and developed some dfppy-based iridium(III) complexes, e.g., FIr6 [31,32], FIrtaz and $FIrN_4$ [33]. In order to achieve true-blue and near-UV phosphorescence emission, pyridylazole- and carbene-based iridium(III) complexes were developed by Chi et al. [34–37], Thompson et al. [38,39], respectively. All these complexes with molecular formula $[Ir(C\hat{}N)_3]$ or $[Ir(C\hat{}N)_2(L\hat{}X)]$ (C^N and L^X stand for cyclometalated ligand and anionic ancillary ligand, respectively) are neutral, and most of the OLEDs based on these complexes were fabricated by vacuum deposition technique due to their good volatility. However, this greatly increases the complexity of OLED process technologies and manufacturing costs. Recently, cationic blue-emitting iridium(III) complexes $[Ir(C\hat{}N)_2(L\hat{}L')]^+$ (L^L′ stands for neutral ancillary ligand) have been developed and corresponding light-emitting electrochemical cells (LECs) [40–44], a new type of organic electroluminescent device, were fabricated due to their good thermal and photophysical stabilities. In this research direction, our group have been interested in design and synthesis of blue- and blue–green-emitting cationic iridium(III) complexes in order to meet the necessary requirements of full-color display and solid-state lighting applications. Some cationic iridium(III) complexes, e.g., $[Ir(ppy)_2(pzpy)]PF_6$, $[Ir(dfppy)_2(pzpy)]PF_6$, $[Ir(ppy)_2(bid)]PF_6$, $[Ir(dfppy)_2(pyim)]PF_6$ and $[Ir(dfppz)_2(tp\text{-}pyim)]PF_6$, were synthesized and LECs based on these complexes were fabricated, which gave blue and blue–green electroluminescence [45–47]. Taking into account the good solubilities in organic solvents and excellent film-forming properties doped in polymers, we fabricated solution-processed OLEDs based on these complexes [48,49]. Our work indicated that the ionic nature of these complexes is beneficial in reducing aggregations of dopants in the polar host and thus producing less severe triplet–triplet annihilations at high current densities. Moreover, in comparison with the vacuum evaporation, the solution processing technique to fabricate OLEDs greatly simplified the manufacturing process and reduced manufacturing costs. Along this line of research, we report here photophysical and electrochemical properties of two new cationic iridium complexes $[Ir(ppy)_2(pymi)]PF_6$ (**1**) and $[Ir(dfppy)_2(pymi)]PF_6$ (**2**) (Scheme 1), based on 1-pyridyl-3-methylimidazolin-2-ylidene-C,$C^{2'}$ (pymi) as the ancillary ligand containing a carbene moiety. Carbene moiety is a neutral, two electron donor, and can afford a much stronger ligand-to-metal dative interaction. Complex **1** and complex **2** show blue light emission (472 and 451 nm, respectively), in degassed CH_3CN solutions, which exhibit slightly blue-shift with respect to our previously reported complexes $[Ir(ppy)_2(pzpy)]PF_6$ (475 nm) and $[Ir(dfppy)_2(pzpy)]PF_6$ (452 nm) [45], respectively. Although LECs based on cationic iridium complexes with carbene derivatives as ancillary ligands were reported [44,50], to the best of our knowledge, there is no report on corresponding OLEDs till now. Complexes **1** and **2** are suitable for solution processing to make doped polymer films due to their good solubilities in organic solvents. Therefore, solution-processed OLEDs using complexes **1** and **2** as dopants in poly(N-vinylcarbazole) (PVK) were fabricated and exhibit efficient blue–green electrophosphorescence with maximum efficiencies of 5.2 and 0.85 cd A^{-1}, maximum brightnesses of 5249 and 906 cd m^{-2}, CIE (Commission Internationale de l'Éclairage) coordinates of (0.21, 0.45) and (0.21, 0.33), respectively.

2. Experimental

2.1. General experiments

All reactants and solvents were used as received, and were purified or dried by standard methods when required. ^{1}H-NMR spectra were recorded on a JOEL JNM-ECA600 NMR spectrometer with tetramethylsilane (TMS) as the internal standard. Mass spectrometry was performed with an Esquire-LC_00136 mass spectrometer. Elemental analysis for carbon, hydrogen and nitrogen were determined on an Exeter Analytical CE-440 Elemental Analyzer. UV absorption spectra were obtained from CH_3CN solutions were recorded with a UV–vis spectrophotometer (Agilent 8453). PL spectra were recorded with a fluorospectrophotometer (Jobin Yvon, FluoroMax-3). The PL decay lifetimes were recorded on a transient spectrofluorimeter (Edinburgh Instruments, FLSP920) with a time-correlated single-photon counting technique. The photoluminescent quantum yields (PLQYs) of the complexes were measured in degassed CH_3CN solutions with quinine sulfate (Φ_p = 0.545 in 1 M H_2SO_4) as the standard [51]. The solutions were degassed by three freeze–pump-thaw circles before measurements. The PLQYs in thin films were measured with an integrating sphere on a fluorospectrophotometer (Jobin Yvon, FluoroMax-3) according to a reported procedure [52]. Cyclic voltammetry was performed on a Princeton Applied Research potentiostat/galvanostat model 283 voltammetric analyzer in CH_3CN solutions (2×10^{-3} M) at a scan rate of 100 mV/s, with a platinum plate as the working electrode, a silver wire as the reference electrode and a platinum wire as the counter electrode. The supporting electrolyte was tetrabutylammonium hexafluorophosphate (0.1 M) and ferrocene (Fc) was used as the internal standard. The solutions were degassed with argon before measurements.

2.2. Preparation and composition analysis

Synthesis of 1-pyridyl-3-methylimidazolium bromide ($pymi^+Br^-$). This ligand was synthesized by a previously reported procedure with a yield of 38% [53].

Synthesis of $[Ir(ppy)_2(pymi)]PF_6$ (**1**). The cationic iridium complex $[Ir(ppy)_2(pymi)]PF_6$ was synthesized according to the reference [50]. A mixture of $pymi^+Br^-$ (0.48 g, 2 mmol), Ag_2O (0.92 g, 4 mmol), and the dichloro-bridged cyclometalated iridium complex $[(ppy)_2Ir(\mu\text{-}Cl)]_2$ (1.07 g, 1 mmol) in 2-ethoxyethanol (30 mL) was heated to reflux at 130 °C for 12 h in the dark. After cooling to room temperature, the solution was filtered through a sintered-glass frit and an excess (10 equiv) of NH_4PF_6 (in 100 mL of H_2O) was added to induce precipitation. The yellow precipitate was collected by filtration, washed with

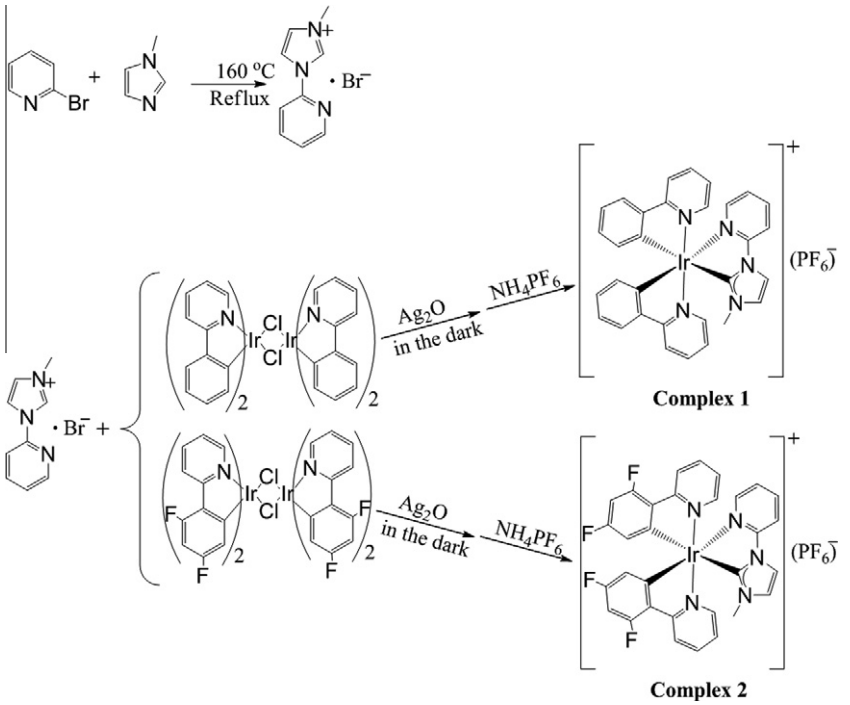

Scheme 1. The synthetic routes and structures of complex **1** and complex **2**.

excess H_2O, and then dried under vacuum. The solid was separated using silica gel column chromatography (CH_2Cl_2/CH_3OH = 50:1), giving a light-yellow complex **1** (1.03 g, 1.28 mmol, 64% yield). ^1H NMR (600 MHz, acetone-d_6, δ): 8.36 (d, J = 2.0 Hz, 1H), 8.29 (d, J = 8.2 Hz, 1H), 8.23 (m, 4H), 7.95 (t, J = 8.2 Hz and 7.6 Hz, 2H), 7.88 (t, J = 7.6 Hz and 6.2 Hz, 2H), 7.84 (t, J = 6.8 Hz and 6.2 Hz, 2H), 7.46 (m, 2H), 7.15 (m, 2H), 7.04 (t, J = 7.6 Hz, 1H), 6.95 (m, 2H), 6.84 (t, J = 6.8 Hz and 8.3 Hz, 1H), 6.46 (d, J = 7.6 Hz, 1H), 6.30 (d, J = 7.6 Hz, 1H), 3.29 (s, 3H). ESI-MS [m/z]: 660.2 $(M-PF_6)^+$. Anal. found: C 46.54, H 3.17, N 8.45. Anal. Calcd. for $C_{31}H_{25}N_5PF_6Ir$: C 46.27, H 3.13, N 8.70.

Synthesis of $[Ir(dfppy)_2(pymi)]PF_6$ (**2**). The synthesis of complex **2** was similar to that of complex **1** except that the dichloro-bridged cyclometalated iridium complex $[(ppy)_2Ir(\mu\text{-}Cl)]_2$ was replaced with $[(dfppy)_2Ir(\mu\text{-}Cl)]_2$. Yield: 68%. ^1H NMR (600 MHz, acetone-d_6, δ): 8.36 (m, 6H), 8.06 (m, 2H), 7.95 (d, J = 5.5 Hz, 1H), 7.92 (d, J = 5.5 Hz, 1H), 7.56 (s, 1H), 7.52 (m, 1H), 7.23 (m, 2H), 6.73 (m, 2H), 5.90 (m, 1H), 5.73 (m, 1H), 3.41 (s, 3H). ESI-MS [m/z]: 732.2 $(M-PF_6)^+$. Anal. found: C 42.30, H 2.43, N 7.70. Anal. Calcd. for $C_{31}H_{21}N_5PF_{10}Ir$: C 42.47, H 2.41, N 7.99.

2.3. X-ray crystallography

Single crystals of complexes **1** and **2** were grown from slow evaporation of ethanol/acetone (1:1) solutions. The room temperature single-crystal X-ray experiments were performed on a RIGAKU SATURN 724+CCD diffractometer equipped with a graphite monochromatized Mo K_α radiation. The structures were solved by direct methods and refined with a full-matrix least-squares technique based on F^2 with the SHELXL-97 crystallographic software package [54].

Selected Crystal Data of complex **1**: Space group *Pbca* with a = 11.016(2) Å, b = 16.330(3) Å, c = 31.732(6) Å, α = 90.00°, β = 90.00°, γ = 90.00°, V = 5709(2) Å^3, Z = 8, d_{calcd} = 1.873 g cm^{-3}, R_1 = 0.0436, ωR_2 = 0.1143 for 5105 observed reflections [$I \geq 2\sigma(I)$]. Selected Crystal Data of complex **2**: Space group $P2_1/c$ with a = 14.740(3) Å, b = 25.102 (5) Å, c = 9.3763(19) Å, α = 90.00°, β = 107.08(3)°, γ = 90.00°, V = 3316.2(11) Å^3, Z = 4, d_{calcd} = 1.870 g cm^{-3}, R_1 = 0.0353, ωR_2 = 0.0703 for 5820 observed reflections [$I \geq 2\sigma(I)$]. More crystallographic data can be found in CCDC 856217 and CCDC 856218, which can be obtained free of charge from the Cambridge Crystallographic Data Center from http://www.ccdc.cam.ac.uk/conts/retrieving.html.

2.4. Quantum chemical calculations

Density functional theory (DFT) and time-dependent DFT (TD-DFT) calculations on the ground and excited electronic states of complex **1** and complex **2** were carried out at the B3LYP level [55,56]. "Double-ξ" quality basis sets were employed for the C, H, N, and F (6-31G**) and the Ir (LANL2DZ). An effective core potential (ECP) replaces the inner core electrons of Ir leaving the outer core $(5s)^2(5p)^6$ electrons and the $(5d)^6$ valence electrons of Ir(III). The initial ground-state geometries were directly obtained from the X-ray single-crystal structures. The geometries of the singlet ground state (s_0) were fully optimized with C1 symmetry constraints. All calculations were performed with Gaussian 03 software package using a spin-restricted formalism [57].

2.5. Fabrication and characterization of OLEDs

Indium-tin-oxide (ITO) substrates with sheet resistance of 15 Ω/□ were sufficiently cleaned using chemical and UV-ozone methods before the deposition of the organic layers. The poly-(3,4-ethylenedioxy-thiophene:poly-(styrene sulfonate) (PEDOT:PSS) layer was spin-coated onto the ITO substrate in air and baked at 200 °C for 10 min. The light-emitting layers was then spin-coated onto the PEDOT:PSS-coated substrate from a mixed solution of poly(N-vinylcarbazole) (PVK): 1,3-bis(5-(4-tert-butylphenyl)-1,3,4-oxadiazol-2-yl)benzene (OXD-7): complex **1** (or complex **2**) in 1,2-dichloroethane in a nitrogen atmosphere glove box and baked at 80 °C for 30 min. The substrate was then transferred into an evaporation chamber, where the 1,3,5-tris[N-(phenyl)benzimidazole]-benzene (TPBI) was evaporated at an evaporation rate of 1–2 Å/s under a pressure of 4×10^{-4} Pa and the Cs_2CO_3/Al bilayer cathode was evaporated at evaporation rates of 0.2 and 8–10 Å/s for Cs_2CO_3 and Al, respectively, under a pressure of 1×10^{-3} Pa. The current–voltage–brightness characteristics of the devices were recorded with Keithley 4200 semiconductor characterization system. The electroluminescent spectra were collected with a Photo Research PR705 Spectrophotometer. All measurements of the devices were carried out in ambient atmosphere without further encapsulations.

3. Results and discussion

3.1. Synthesis and structural characterization

Scheme 1 shows the synthetic routes and structures of complexes **1** and **2**. The ancillary proligand pymi$^+$Br$^-$ was readily synthesized from the reaction of 2-bromopyridine with 1-methylimidazole keeping neat at 160 °C for 48 h according to the general procedure of Concepcion et al. reported [53]. The reaction of pymi$^+$Br$^-$ with the chloro-bridged dimers [(ppy)$_2$Ir(μ-Cl)$_2$Ir(ppy)$_2$] and [(dfppy)$_2$Ir(μ-Cl)$_2$Ir(dfppy)$_2$] in 2-ethoxyethanol using silver(I) oxide as catalyst followed by a counter ion-exchange reaction

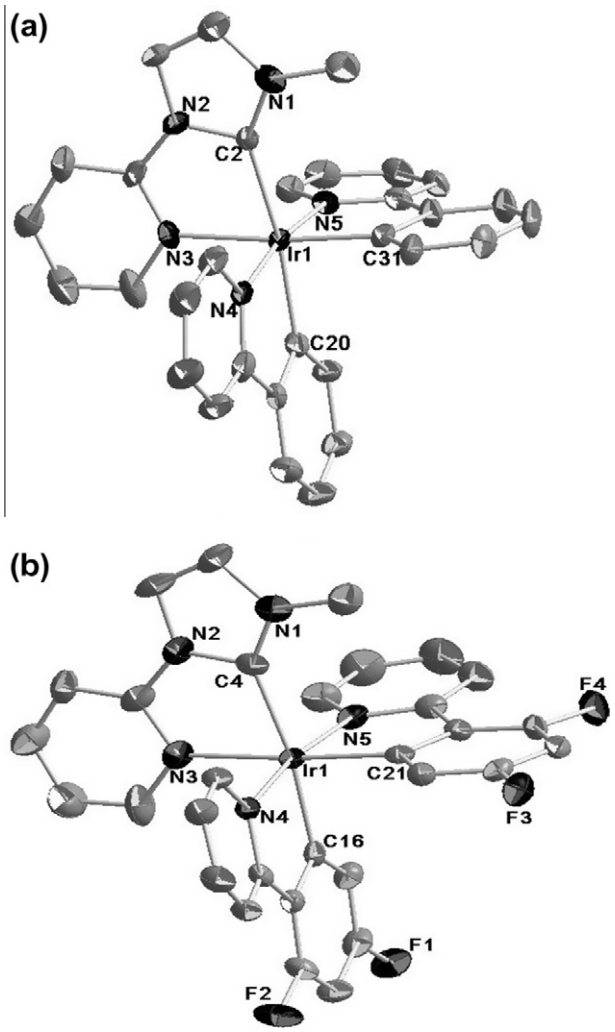

Fig. 1. Crystal structures of complexes **1** (a) and **2** (b). Thermal ellipsoids are drawn at 50% probability. The PF_6^- counter anions, solvent molecules, and H atoms have been omitted for clarity.

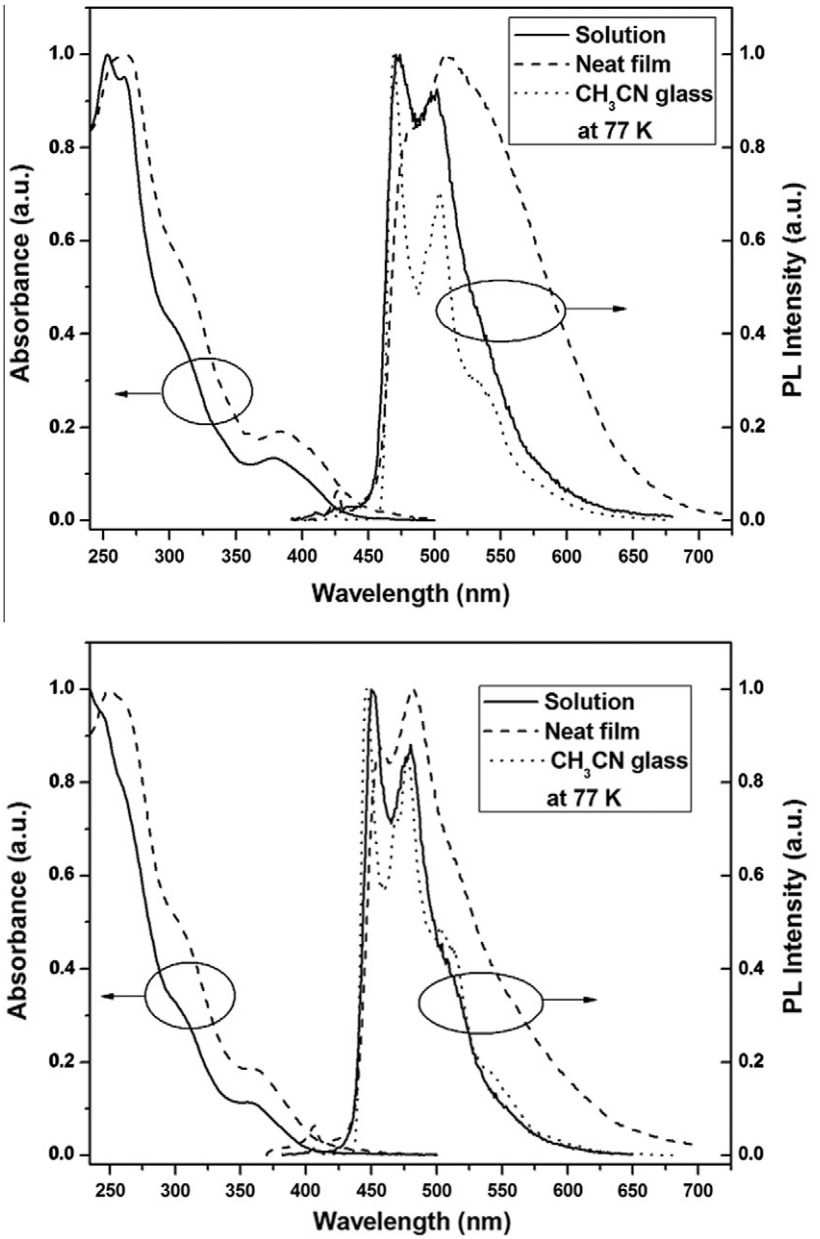

Fig. 2. Absorption and emission spectra of complexes **1** (top) and **2** (bottom) in dilute CH_3CN solutions and neat films.

from Br^- to PF_6^- yielded complexes **1** and **2**, respectively, according to the literature method [50]. These complexes were fully structurally characterized by ESI (electron spray ionization) mass spectroscopy, NMR and elemental analysis (see Experimental Section).

To further confirm their molecular structures, single crystals of complexes **1** and **2** were grown from slow evaporation of methanol/acetone solutions and characterized using X-ray crystallography (see Experimental Section). As shown in Fig. 1, these complexes exhibit distorted octahedral geometries of three nitrogens and three carbons from the cyclometalated ligands and pymi ancillary ligand in a meridional arrangement. In complex **1**, the Ir-N bonds of the mutually trans pyridyl groups (Ir-N4 = 2.055(5) Å and Ir-N5 = 2.045(5) Å) are similar to those of complex **2** (Ir-N4 = 2.051(4) Å and Ir-N5 = 2.044(4) Å). The bond lengths of Ir-C_{ppy} and Ir-C_{dfppy} trans to carbene moiety (Ir-C20 = 2.039(7) Å and Ir-C16 = 2.038(5) Å, respectively) are significantly greater than those of both Ir-C trans to the pyridyl groups (Ir-C31 = 2.013(6) Å and Ir-C16 = 2.015 (5) Å, respectively) and Ir-C_{ppz} trans to pyrazolyl group in *mer*-Ir$(ppz)_3$ (Ir-C3 = 1.993(2) Å) [39], illustrating the stronger trans influence of the carbene group than those of pyridyl and pyrazolyl moieties.

Table 1
Photophysical characteristics of complexes **1** and **2** in CH_3CN solutions.

	λ_{abs} (nm) (ε [10^4 M^{-1} cm^{-1}])[a]	PL at room temperature[b]		PL at 77 K[c]	
		λ_{em} (nm)	Φ_{PL} [τ (μs)]	λ_{em} (nm)	τ (μs)
1	253 (5.36), 381 (0.69), 408 (0.40)	472, 501 (sh)	0.0052 [0.032]	470, 504 (sh), 532 (sh)	4.32
2	247 (5.15), 359 (0.61), 395 (0.16)	451, 480 (sh)	0.0086 [0.072]	446, 477 (sh), 503 (sh)	4.94

[a] In 1×10^{-5} M CH_3CN solution.
[b] In degassed CH_3CN solution; the symbol sh denotes the shoulder wavelength.
[c] In CH_3CN glass at 77 K.

Table 2
Photophysical characteristics in thin films and electrochemical characteristics in solutions of complexes **1** and **2**.

	Neat film[a]		5 wt.% doped PMMA film[a]	Electrochemical data[c]	
	λ_{em} (nm)	Φ_{PL} [τ (μs)][b]	Φ_{PL} [τ (μs)][b]	E_{ox} (V)	E_{red} (V)
1	480 (sh), 508	0.24 [0.31 (33%) 0.043 (67%)]	0.26 [2.74 (65%) 0.94 (35%)]	0.82	−2.40
2	457 (sh), 482	0.073 [0.39 (31%) 0.092 (69%)]	0.23 [3.67 (82%) 0.88 (18%)]	1.20	−2.30

[a] Films were deposited on quartz substrates with thicknesses of about 100 nm.
[b] The percentage in parentheses denotes the percentage of each lifetime.
[c] In degassed 2×10^{-3} M CH_3CN solutions. Potentials were recorded versus Fc^+/Fc.

3.2. Photophysical properties

The absorption and PL spectra of complexes **1** and **2** in dilute CH_3CN solutions and thin films are shown in Fig. 2 and detailed photophysical characterizations are summarized in Tables 1 and 2. The strong absorption bands in the ultra-violet up to around 350 nm attributed to spin-allowed $\pi \rightarrow \pi^*$ transitions from the ligands. The relatively weak absorption bands from 350 nm extending to the visible region are assign to excitations to ^{1}MLCT (metal-to-ligand charge-transfer), ^{1}LLCT (ligand-to-ligand charge-transfer), ^{3}MLCT, ^{3}LLCT, and ligand-centered (LC) $^3\pi \rightarrow \pi^*$ transitions [45].

As depicted in Fig. 2, complexes **1** and **2** exihibit blue light emission (475 and 451 nm, respectively) in degassed CH_3CN solutions at room temperature, which exhibit slightly blue-shift with respect to our previously reported complexes $[Ir(ppy)_2(pzpy)]PF_6$ (475 nm) and $[Ir(dfppy)_2(pzpy)]PF_6$ (452 nm) [45]. respectively. Both complex **1** and complex **2** exhibit structured emission spectra, which can be fitted by the Huang–Rhys factor, S, of 0.92 and 0.87, respectively [58]. This indicates that the structure of emission spectra is due to the different vibrational levels of the ground states. At 77 K in CH_3CN glass, both complex **1** and complex **2** show much more structured emission spectra (Fig. 2), which present little rigidochromic blue-shifts (4–6 nm) with respect to their emission spectra at room temperature. For complex **1**, the photoluminescence lifetime of 32 ns was obtained, from which the radiative lifetime is estimated as 6.15 μs using the measured PLQY of 0.0052. Similarly, the radiative lifetime of complex **2** was deduced to be 8.37 μs, confirming their phosphorescence origin in nature.

In degassed CH_3CN solution, complexes **1** and **2** exhibit low photoluminescence quantum yields (PLQYs) of 0.0052 and 0.0086, respectively, as have been observed for the previously reported pyridine-carbene based iridium complexes [44]. The low PLQYs of these complexes are attributed to non-negligible non-radiative process (energy transfer) to solvent with PF_6 anion. This is confirmed by observation of much higher PLQY in film (vide infra), and also by previous observation that no PLQY difference between solution and film for non-cationic phosphors like PtOEP and $Ir(ppy)_3$ [59,60].

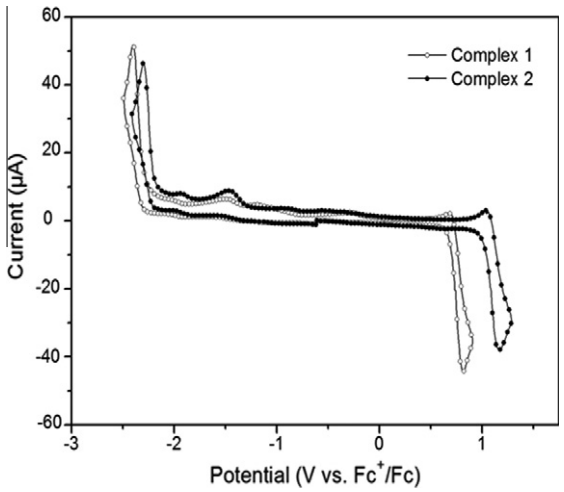

Fig. 3. Cyclic voltammograms of complexes **1** and **2** in CH_3CN solutions (10^{-3} M). Potentials were recorded versus Fc^+/Fc.

As depicted in Fig. 2, the emission maxima of complexes **1** and **2** in neat films are 508 and 482, respectively. Compared with the peaks at 472 and 451 nm in solution, the intensities at 480 and 457 nm in neat films are significantly decreased with small red-shifts (6–8 nm). This phenomenon for PL spectra in neat films are related to both self-absorption and strong intermolecular interactions [61]. In sharp contrast to the PLQYs in solutions, the doped films of complexes **1** and **2** in polymer poly(methyl methacrylate) (PMMA) exhibit significantly better PLQYs of 0.26

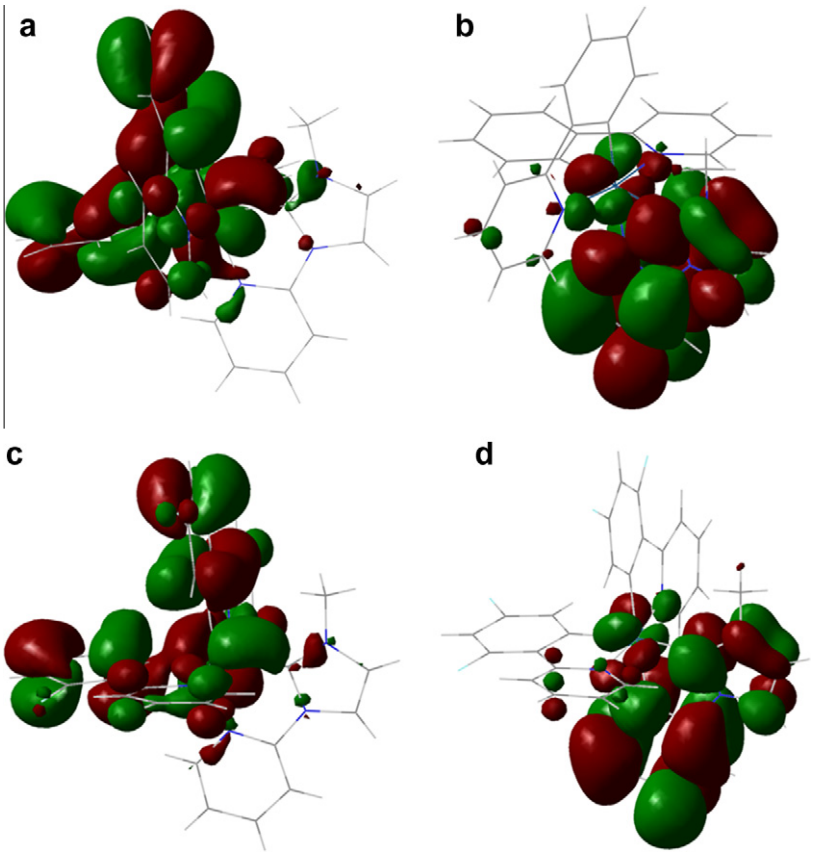

Fig. 4. Molecular orbital surfaces of cationic iridium complexes. (a) HOMO orbital of complex **1**. (b) LUMO orbital of complex **1**. (c) HOMO orbital of complex **2**. (d) LUMO orbital of complex **2**. All the MO surfaces correspond to an isocontour value of $|\psi| = 0.02$.

Table 3
Selected triplet states for complex **1** and complex **2** calculated from TDDFT approach.

	States	E[a] (eV)	Dominant excitations[b]	Nature
1	T1	2.69	H → L (0.97)	dπ(Ir)-π(ppy) → π*(pymi)
	T2	2.79	H-1 → L+1 (0.22)	dπ(Ir)-π(ppy) → π*(ppy)-π*(pymi)
			H → L+1 (0.39)	dπ(Ir)-π(ppy) → π*(ppy)-π*(pymi)
	T3	2.88	H → L + 3 (0.49)	dπ(Ir)-π(ppy) → π*(ppy)
2	T1	2.89	H → L (0.82)	dπ(Ir)-π(dfppy) → π*(pymi)
	T2	2.96	H-1 → L+1 (0.25)	dπ(Ir)-π(dfppy) → π*(dfppy)-π*(pymi)
			H → L (0.19)	dπ(Ir)-π(dfppy) → π*(pymi)
			H → L+1 (0.19)	dπ(Ir)-π(dfppy) → π*(dfppy)-π*(pymi)
	T3	3.07	H-2 → L+3 (0.30)	dπ(Ir)-π(dfppy) → π*(dfppy)
			H → L+3 (0.30)	dπ(Ir)-π(dfppy) → π*(dfppy)

[a] Excitation energies calculated for the triplet states.
[b] H and L denote HOMO and LUMO, respectively; data in parentheses are the contributions of corresponding excitations.

and 0.23, respectively, accompanied by a remarkable increase of excited state lifetimes (Table 2). This enhancement in quantum yield and excited state lifetime plausibly result from the great restriction of rotations and vibrations in rigid polymer [62].

3.3. Electrochemical properties

The electrochemical properties of complex **1** and complex **2** were investigated by means of cyclic voltammetry (CV) mesaurement by using ferrocene as intermal standard, and the redox potentials are listed in Table 2. As shown in Fig. 3, complex **1** and complex **2** both show quasi-reversible oxidation processes and irreversible reduction processes in CH_3CN solutions. The oxidation potential of complex **1** (0.82 V) is almost the same as those of other ppy based iridium complexes [45,62]. It is confirmed that the oxidation occurred mainly at the iridium metal center. The oxidation potential (1.20 V) of complex **2** is largely shifted anodically compared to that of complex **1**, indicating that the HOMO of

complex **2** is significantly stabilized by introducing the electron-withdrowing F substituents on the phenyl rings. At the same time, the reduction potential of complex **2** (−2.30 V) is slightly shifted cathodically compared to that of complex **1** (−2.40 V).

3.4. Quantum chemical calculations

DFT calculations at the B3LYP/(6-31G**+LANL2DZ) level were carried out to gain more insight into the photophysical and electrochemical properties of the complex **1** and complex **2** (see Experimental Section). Electronic ground states of complex **1** and complex **2** were directly calculated based on the geometries obtained from their single-crystal structures. Fig. 4 displays the atomic orbital composition of the HOMOs and LUMOs for complexes **1** and **2**. As expected, the HOMO orbitals of all complexes were composed of a mixture of Ir dπ orbitals and phenyl π orbitals distributed among the cyclometalated ligands, while their LUMO orbitals were mainly located on the pymi ancillary ligands. For complexes **1** and **2**, HOMO-1 and HOMO-2 orbitals still resided on the cyclometalated ligands (mainly on the phenyl groups) and the iridium ions with small changes of the atomic orbital composition. However, their LUMO+1 and LUMO+2 orbitals were mainly located on the pyridine rings of both the cyclometalated ligands and pymi ancillary ligands, and LUMO+3 orbitals only resided on the pyridine rings of the cyclometalated ligands. The calculated energy gaps (LUMO–HOMO) of complexes **1** and **2** are 3.43 eV and 3.63 eV, respectively, which are consistent with the experimentally obtained electrochemical band gaps (3.22 eV and 3.50 eV, respectively).

Complex **1** and complex **2** have the same pymi ancillary ligands on which their LUMOs are localized, which provides the rationale for nearly the same reduction potentials (−2.40 and −2.30 V, respectively). However, owing to the present of the electron-withdrawing fluorine atoms which sequently stabilizes the HOMO, complex **2** shows the anodically shifted oxidation potential and blue-shifted emission spectra relative to complex **1**.

To further confirm the nature of the emitting exicited state, DFT calculations were performed to determine the low-lying triplet states of complex **1** and complex **2**. Table 3 summarizes the vertical excitation energies and orbitals involved in the excitations for calculated triplets below 3.10 eV. TDDFT calculations predict that the low-lying triplet states shows a similar nature for complex **1** and complex **2**, and calculated T_1, T_2, and T_3 states are relatively close in energy (within 0.19 and 0.18 eV, respectively) and, in principle, emission might occur from any of them [63]. For the two complexes, the T_1 states mainly result from the HOMO → LUMO monoexcitation, which correspond to the ^{3}MLCT (dπ(Ir) → π*(pymi)) and ^{3}LLCT (π(ppy) or π(dfppy) → π*(pymi)) characters. However, the T_2 states mainly originate the HOMO-1 → LUMO+1 and HOMO → LUMO+1, which correspond to the ^{3}LC π → π* (π(ppy) or π(dfppy) → π*(ppy) or π*$^{(dfppy))}$, ^{3}MLCT (dπ(Ir) → π*(pymi)) and ^{3}LLCT (π(ppy) or π(dfppy) → π*(pymi)) characters. The T_3 states mainly originate the HOMO → LUMO+3 and HOMO-2 → LUMO+3, which correspond to the nature of ^{3}LC π → π* (π(ppy) or π(dfppy) → π*(ppy) or π*(dfppy)) with some ^{3}MLCT (dπ(Ir) → π*(pymi)) character. By taking into account the observed structured emission spectra (Fig. 2) and fast nonradiative multi-phonon (NMP) transitions from the upper T2 and T3 levels to the lowest T1 levels, it can be concluded that the observed spectra are due to the transition from the T1 states.

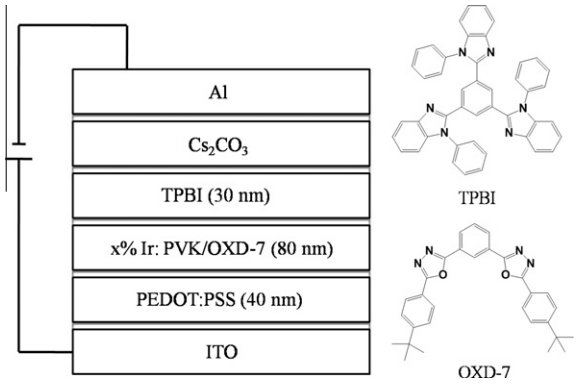

Fig. 5. Device architecture and chemical structures of the materials used in these OLEDs.

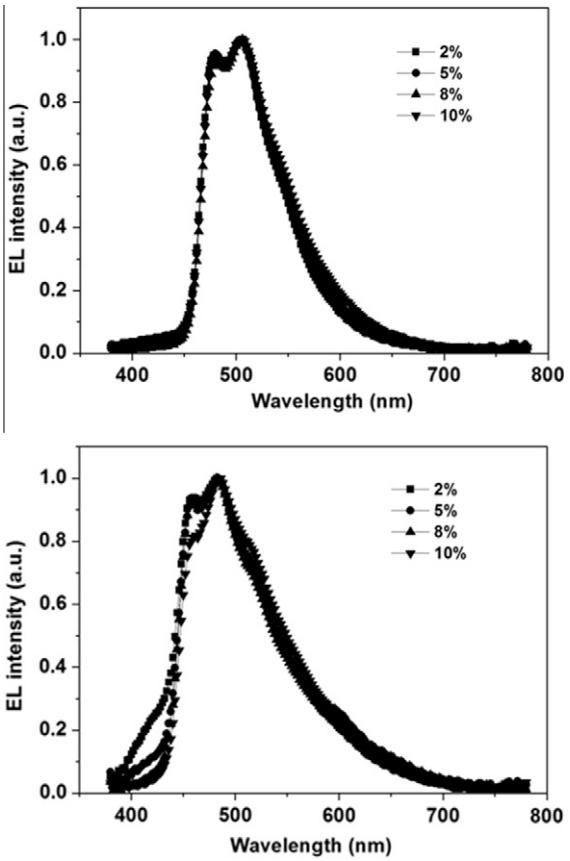

Fig. 6. EL spectra of the OLEDs based on complexes **1** (top) and **2** (bottom) at different doping concentrations (under 7 V).

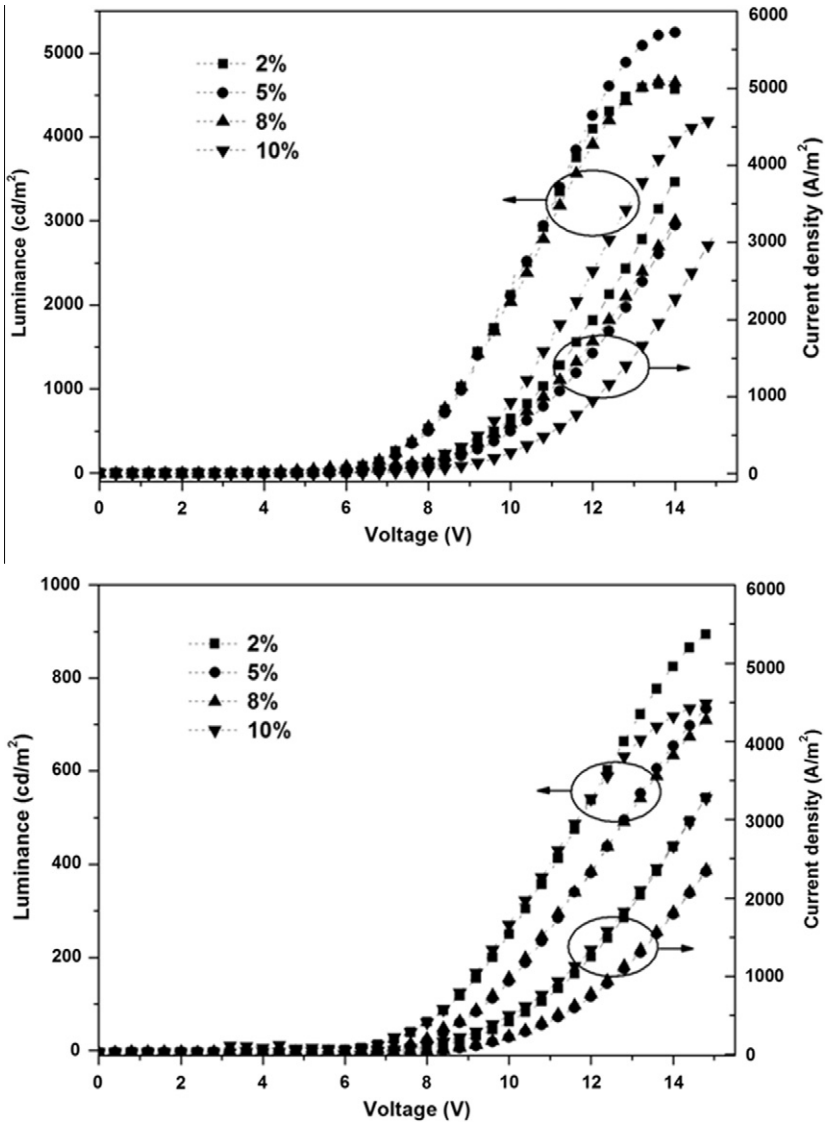

Fig. 7. The luminance-voltage-current density characteristics of the OLEDs based on complexes **1** (top) and **2** (bottom) at different doping levels.

Table 4
Electrical characteristics of devices based on complexes **1** and **2**.

Phosphor dopant	$V_{turn\text{-}on}$ (V)	L_{max} (cd m^{-2}, V)[a]	η_L (cd A^{-1}, V)[a]	λ_{em} (nm)	CIE (*x*,*y*)
1 (2 wt.%)	4.2	4629, (13.6)	4.1, (7.1)	506	(0.21, 0.45)
1 (5 wt.%)	4.9	5249, (14.0)	5.2, (7.4)	506	(0.22, 0.46)
1 (8 wt.%)	5.1	4667, (13.7)	3.6, (9.2)	506	(0.22, 0.46)
1 (10 wt.%)	6.0	4203, (15.0)	3.6, (8.3)	506	(0.24, 0.46)
2 (2 wt.%)	6.0	906, (15.0)	0.85, (7.7)	482	(0.22, 0.30)
2 (5 wt.%)	6.0	748, (15.0)	0.85, (8.5)	483	(0.23, 0.35)
2 (8 wt.%)	6.2	726, (15.0)	0.82, (8.4)	482	(0.21, 0.33)
2 (10 wt.%)	7.0	748, (15.0)	0.57, (8.8)	483	(0.24, 0.35)

[a] Maximum values of the devices. Values in parentheses are the voltages at which they were obtained.

3.5. Electroluminescent properties of OLED devices

In order to evaluate the electroluminescent properties of these complexes, **1** and **2** were employed as doped emitters to fabricate the OLEDs by solution process. The device architecture and chemical structures of the materials used are shown in Fig. 5. PEDOT:PSS acts as hole-injecting layer. To facilitate electron transport in the light-emitting layers,

OXD-7 is mixed into the PVK as co-host. TPBI acts as both an exciton-blocker and an electron-transporter, and Cs_2CO_3/Al as the electron-injection layer and cathode. For optimization purposes, the doping level of each iridium phosphor was varied at four different concentrations (2%, 5%, 8% and 10%, respectively).

Fig. 6 depicts the EL spectra of the OLEDs based on complexes **1** and **2** at different doping concentrations (under 7 V). Devices based on complex **1** as the dopant show bright blue–green light emission with the emission peak at about 506 nm and a shoulder peak at 480 nm. The Commission International de L'Eclairage (CIE) color coordinates of the four devices vary a little from (0.21, 0.45) to (0.24, 0.46) and the turn-on voltage ($V_{\text{turn-on}}$) are about 4.2–6.0 V. Furthermore, in the EL spectra, the emission from PVK: OXD-7 (around 410 nm) disappears completely even at low doping concentrations, indicating that the complete energy transfer occurs from PVK: OXD-7 to the complex **1**. Devices based on complex **2** exhibit blue–green light emission with the emission peak at about 484 nm and a shoulder peak at 458 nm. The CIE color coordinates of the four devices vary a little from (0.21, 0.33) to (0.24, 0.35), which present much blue-shift with respect to the electrophosphorescence based on complex **1**. However, at low doping concentrations of the dopant (2% and 5%), the weak emission from PVK: OXD-7 was observed, indicating incomplete energy transfer from PVK: OXD-7 to complex **2**. With the increase of doping concentration, emission from PVK: OXD-7 is disappeared, and accompanied by a decrease in the intensity of the shoulder peak at 458 nm. In addition, the emission wavelengths of EL spectra of complexes **1** and **2** closely resemble those of PL spectra in solutions or thin films, indicating that electroluminescence originated from the doped cationic iridium complexes **1** and **2** [45,49].

Fig. 7 shows the luminance-voltage-current density characteristics of devices with different doping concentrations of complexes **1** and **2**. Detailed electrical characteristics of the devices are summarized in Table 4. As depicted in Fig. 7, the best performances of the devices are achieved at the low doping level of 5 wt.% for complex **1** and 2 wt.% for complex **2**. For complex **1**, a maximum luminance (L_{max}) of 5249 cd m^{-2} at 14 V and a maximum luminance efficiency (η_L) of 5.2 cd A^{-1} at 7.4 V are achieved at a doping concentration of 5 wt.%. For complex **2**, a maximum luminance (L_{max}) of 906 cd m^{-2} at 15 V and a maximum luminance efficiency (η_L) of 0.85 cd A^{-1} at 7.7 V are achieved at a doping concentration of 5 wt.%. The devices based on complex **2** exhibit inferior electroluminescent properties compared with those of complex **1**. This is mainly because that the HOMO level of complex **2** (−5.9 eV) is much lower than those of complex **1** (−5.6 eV) and the host PVK (−5.8 eV) due to the fluorine atoms attached to the cyclometalated ligands in complex **2** (Fig. 8). In the devices doped with complex **2**, holes cannot be easily injected into the HOMO of complex **2** from PVK, which leads to difficulties of combination with electrons to form excitons along the HOMOs. This phenomenon resemble our previously reported devices doped with pyrazole and imidazole based cationic iridium complexes [48,49]. Fig. 9 shows the dependence of the luminance

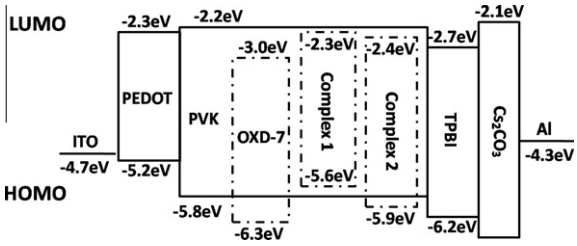

Fig. 8. Energy level (unit: eV) diagrams of the devices. The HOMO and LUMO levels of complexes **1** and **2** were calculated from their redox potentials.

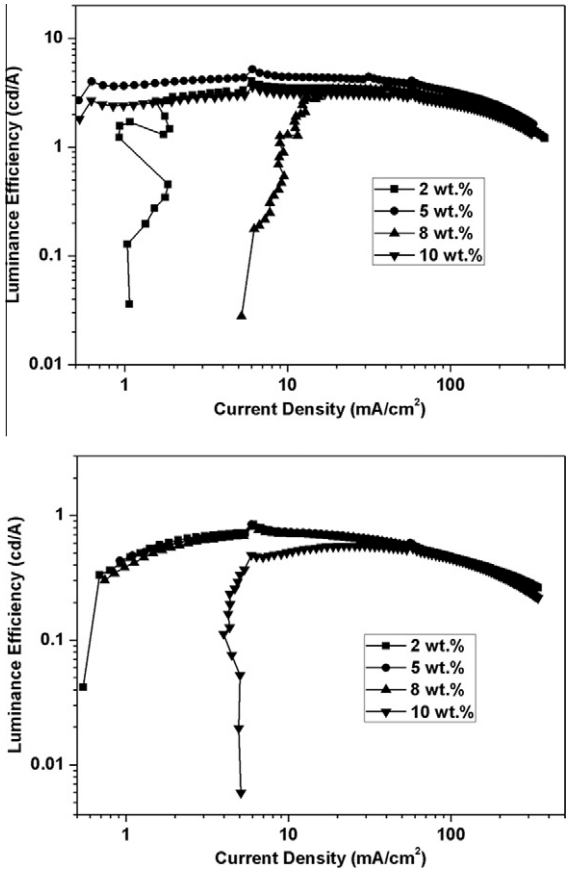

Fig. 9. The luminance efficiency-current density characteristics of the OLEDs based on complexes **1** (top) and **2** (bottom) at different doping levels.

efficiency–current density characteristics of devices based on complexes **1** and **2** at different doping concentrations. As depicted in Fig. 9, these devices exihibit very low roll-off at high current densities, which is also observed in other phosphorescent OLEDs based on cationic iridium complexes [49]. The PF_6^- anions in the lattice can separate the cations so as to reduce aggregations of dopants in the polar host, which may play a role in reducing efficiency roll-off in devices by suppression of triplet–triplet annihilation. It should be noted that the relatively low values

for the luminance and luminance efficiency of the devices based on these complexes compared to those of other cationic iridium complexes [48,49,64] can mainly be attributed to their relatively low photoluminescence quantum yields in solution and film. We firmly believe that the overall performances of the OLEDs are expected to be improved greatly by modifying the ligands of these cationic iridium complexes with appropriate substituents and further optimizing the OLED device structures. Ongoing novel cationic iridium complexes and corresponding device studies are currently in progress.

4. Conclusion

In conclusion, two novel blue-emitting cationic iridium complexes, $[Ir(ppy)_2(pymi)]PF_6$ (**1**) and $[Ir(dfppy)_2(pymi)]PF_6$ (**2**), have been synthesized and fully characterized. With pymi as the ancillary ligand, $[Ir(ppy)_2(pymi)]PF_6$ and $[Ir(dfppy)_2(pymi)]PF_6$ have significantly destabilized LUMO orbitals and, therefore, show blue light emission with the peaks at 472 and 451 nm, respectively, in CH_3CN solution. Due to the good solubilities in organic solvents and excellent film-forming properties doped in polymers, blue–green OLEDs were fabricated by spin coating the emitting layer with these complexes doped in the PVK: OXD-7 host. The maximum efficiency of 5.2 cd A^{-1}, maximum brightness of 5249 cd m^{-2} with CIE coordinates of (0.21, 0.45), respectively, were obtained by using compex **1** as the doped emitter, which suggests that this complex is a promising phosphorescent dopant in solution-processed blue–green OLEDs.

Acknowledgements

We would like to thank the National Key Basic Research and Development Program of China (Grant Nos. 2009CB930602 and 2009CB623604) and the National Natural Science Foundation of China (Grant Nos. 50990060 and 51073089) for financial support.

References

[1] C.W. Tang, S.A. Vanslyke, Appl. Phys. Lett. 51 (1987) 913.
[2] M.A. Baldo, M.E. Thompson, S.R. Forrest, Nature 403 (2000) 750.
[3] S. Lamansky, P. Djurovich, D. Murphy, F. Abdel-Razzaq, H.E. Lee, C. Adachi, P.E. Burrows, S.R. Forrest, M.E. Thompson, J. Am. Chem. Soc. 123 (2001) 4304.
[4] S. Lamansky, P.I. Djurovich, F. Abdel-Razzaq, S. Garon, D.L. Murphy, M.E. Thompson, J. Appl. Phys. 92 (2002) 1570.
[5] B.W. D'Andrade, R.J. Holmes, S.R. Forrest, Adv. Mater. 16 (2004) 624.
[6] N. Rehmann, C. Ulbricht, A. Köhnen, P. Zacharias, M.C. Gather, D. Hertel, E. Holder, K. Meerholz, U.S. Schubert, Adv. Mater. 20 (2008) 129.
[7] H.B. Wu, G.J. Zhou, J.H. Zou, C.L. Ho, W.Y. Wong, W. Yang, J.B. Peng, Y. Cao, Adv. Mater. 21 (2009) 4181.
[8] J.H. Zou, H. Wu, C.S. Lam, C.D. Wang, J. Zhu, C.M. Zhong, S.J. Hu, C.L. Ho, G.J. Zhou, H.B. Wu, W.C.H. Choy, J.B. Peng, Y. Cao, W.Y. Wong, Adv. Mater. 23 (2011) 2976.
[9] G.J. Zhou, W.Y. Wong, S. Suo, J. Photochem. Photobio. C: Photochem. Rev. 11 (2010) 133.
[10] H. Fu, Y.-M. Cheng, P.-T. Chou, Y. Chi, Mater. Today 14 (2011) 472.
[11] M.A. Baldo, D.F. O'Brien, Y. You, A. Shoustikov, S. Sibley, M.E. Thompson, S.R. Forrest, Nature 395 (1998) 151.
[12] M.A. Baldo, S. Lamansky, P.E. Burrows, M.E. Thompson, S.R. Forrest, Appl. Phys. Lett. 75 (1999) 4.
[13] W.Y. Wong, C.L. Ho, Coord. Chem. Rev. 253 (2009) 1709.
[14] W.Y. Wong, C.L. Ho, J. Mater. Chem. 19 (2009) 4457.
[15] G.J. Zhou, W.Y. Wong, X.L. Yang, Chem. Asian J. 6 (2011) 1706.
[16] C.H. Lyons, E.D. Abbas, J.K. Lee, M.F. Rubner, J. Am. Chem. Soc. 120 (1998) 12100.
[17] M. Buda, G. Kalyuzhny, A.J. Bard, J. Am. Chem. Soc. 124 (2002) 6090.
[18] S. Bernhard, X.C. Gao, G.G. Malliaras, H.D. Abruña, Adv. Mater. 14 (2002) 433.
[19] A.R. Hosseini, C.Y. Koh, J.D. Slinker, S. Flores-Torres, H.D. Abruña, G.G. Malliaras, Chem. Mater. 17 (2005) 6114.
[20] N. Armaroli, G. Accorsi, M. Holler, O. Moudam, J.F. Nierengarten, Z. Zhou, R.T. Wegh, R. Welter, Adv. Mater. 18 (2006) 1313.
[21] R.D. Costa, D. Tordera, E. Ortí, H.J. Bolink, J. Schönle, S. Graber, C.E. Housecroft, E.C. Constable, J.A. Zampese, J. Mater. Chem. 21 (2011) 16108.
[22] C.W. Hsu, C.C. Lin, M.W. Chung, Y. Chi, G.H. Lee, P.T. Chou, C.H. Chang, P.Y. Chen, J. Am. Chem. Soc. 133 (2011) 12085.
[23] M. Hashimoto, S. Igawa, M. Yashima, I. Kawata, M. Hoshino, M. Osawa, J. Am. Chem. Soc. 133 (2011) 10348.
[24] W.Y. Wong, Z. He, S.K. So, K.L. Tong, Z.Y. Lin, Organometallics 24 (2005) 4079.
[25] Z. He, W.Y. Wong, X.M. Yu, H.S. Kwok, Z.Y. Lin, Inorg. Chem. 45 (2006) 10922.
[26] G.J. Zhou, Q. Wang, C.L. Ho, W.Y. Wong, D.G. Ma, L.X. Wang, Chem. Commun. (2009) 3574.
[27] G.J. Zhou, Q. Wang, X.Z. Wang, C.L. Ho, W.Y. Wong, D.G. Ma, L.X. Wang, Z.Y. Lin, J. Mater. Chem. 20 (2010) 7472.
[28] P.T. Chou, Y. Chi, M.W. Chung, C.C. Lin, Coord. Chem. Rev. 255 (2011) 2653.
[29] L.X. Xiao, Z.J. Chen, B. Qu, J.X. Luo, S. Kong, Q.H. Gong, J.J. Kido, Adv. Mater. 23 (2011) 926.
[30] C. Adachi, R.C. Kwong, P. Djurovich, V. Adamovich, M.A. Baldo, M.E. Thompson, S.R. Forrest, Appl. Phys. Lett. 79 (2001) 2082.
[31] R.J. Holmes, B.W. D'Andrade, S.R. Forrest, X. Ren, J. Li, M.E. Thompson, Appl. Phys. Lett. 83 (2003) 3818.
[32] X.F. Ren, J. Li, R.J. Holmes, P.I. Djurovich, S.R. Forrest, M.E. Thompson, Chem. Mater. 16 (2004) 4743.
[33] S.J. Yeh, M.F. Wu, C.T. Chen, Y.H. Song, Y. Chi, M.H. Ho, S.F. Hsu, C.H. Chen, Adv. Mater. 17 (2005) 285.
[34] C.H. Yang, Y.M. Cheng, Y. Chi, C.J. Hsu, F.C. Fang, K.T. Wong, P.T. Chou, C.H. Chang, M.H. Tsai, C.C. Wu, Angew. Chem. Int. Ed. 46 (2007) 2418.
[35] Y.H. Song, Y.C. Chiu, Y. Chi, Y.M. Cheng, C.H. Lai, P.T. Chou, K.T. Wong, M.H. Tsai, C.C. Wu, Chem. Eur. J. 14 (2008) 5423.
[36] C.H. Yang, S.W. Li, Y. Chi, Y.M. Cheng, Y.S. Yeh, P.T. Chou, G.H. Lee, C.H. Wang, C.F. Shu, Inorg. Chem. 44 (2005) 7770.
[37] C.-F. Chang, Y.-M. Cheng, Y. Chi, Y.-C. Chiu, C.-C. Lin, G.-H. Lee, P.-T. Chou, C.-C. Chen, C.-H. Chang, C.-C. Wu, Angew. Chem. Int. Ed. 47 (2008) 4542.
[38] R.J. Holmes, S.R. Forrest, T. Sajoto, A. Tamayo, P.I. D'Andrade, M.E. Thompson, J. Brooks, Y.J. Tung, B.W. D'Andrade, M.S. Weaver, R.C. Kwong, J.J. Brown, Appl. Phys. Lett. 87 (2005).
[39] T. Sajoto, P.I. Djurovich, A. Tamayo, M. Yousufuddin, R. Bau, M.E. Thompson, R.J. Holmes, S.R. Forrest, Inorg. Chem. 44 (2005) 7992.
[40] A.B. Tamayo, S. Garon, T. Sajoto, P.I. Djurovich, I.M. Tsyba, R. Bau, M.E. Thompson, Inorg. Chem. 44 (2005) 8723.
[41] M.K. Nazeeruddin, R.T. Wegh, Z. Zhou, C. Klein, Q. Wang, F. De Angelis, S. Fantacci, M. Grätzel, Inorg. Chem. 45 (2006) 9245.
[42] B. Chen, Y. Li, W. Yang, W. Luo, H. Wu, Org. Electron. 12 (2011) 766.
[43] H.C. Su, H.F. Chen, F.C. Fang, C.C. Liu, C.C. Wu, K.T. Wong, Y.H. Liu, S.M. Peng, J. Am. Chem. Soc. 130 (2008) 3413.
[44] F. Kessler, R.D. Costa, D. Di Censo, R. Scopelliti, E. Ortí, H.J. Bolink, S. Meier, W. Sarfert, M. Grätzel, M.K. Nazeeruddin, E. Baranoff, Dalton Trans. 41 (2012) 180.
[45] L. He, L. Duan, J. Qiao, R.J. Wang, P. Wei, L.D. Wang, Y. Qiu, Adv. Funct. Mater. 18 (2008) 2123.
[46] L. He, J. Qiao, L. Duan, G.F. Dong, D.Q. Zhang, L.D. Wang, Y. Qiu, Adv. Funct. Mater. 19 (2009) 2950.
[47] L. He, L.A. Duan, J.A. Qiao, G.F. Dong, L.D. Wang, Y. Qiu, Chem. Mater. 22 (2010) 3535.
[48] L. He, L. Duan, J. Qiao, D.Q. Zhang, G.F. Dong, L.D. Wang, Y. Qiu, Org. Electron. 10 (2009) 152.
[49] L. He, L.A. Duan, J.A. Qiao, D.Q. Zhang, L.D. Wang, Y. Qiu, Org. Electron. 11 (2010) 1185.
[50] C.H. Yang, J. Beltran, V. Lemaur, J. Cornil, D. Hartmann, W. Sarfert, R. Fröhlich, C. Bizzarri, L. De Cola, Inorg. Chem. 49 (2010) 9891.
[51] W.H. Melhuish, J. Phys. Chem. 65 (1961) 229.
[52] L.O. Pålsson, A.P. Monkman, Adv. Mater. 14 (2002) 757.
[53] J.J. Concepcion, J.W. Jurss, M.R. Norris, Z.F. Chen, J.L. Templeton, T.J. Meyer, Inorg. Chem. 49 (2010) 1277.
[54] G.M. Sheldrick, Acta Crystallogr. A64 (2008) 112.

[55] A.D. Becke, J. Chem. Phys. 98 (1993) 5648.
[56] C. Lee, W. Yang, R.G. Parr, Phys. Rev. B 37 (1988) 785.
[57] Gaussian 03, Revision B.05, Gaussian, Inc., Wallingford, CT, 2004.
[58] H. Yersin (Ed.), Highly Efficient OLEDs with Phosphorescent Materials, Wiley-VCH, Weinheim, Germany, 2008, p. 66.
[59] A.K. Bansal, W. Holzer, A. Penzkofer, T. Tsuboi, Chem. Phys. 330 (2006) 118.
[60] W. Holzer, A. Penzkofer, T. Tsuboi, Chem. Phys. 308 (2005) 93.
[61] C. Clementi, C. Miliani, G. Verri, S. Sotiropoulou, A. Romani, B.G. Brunetti, A. Sgamellotti, Appl. Spectrosc. 63 (2009) 1323.
[62] L. He, L. Duan, J. Qiao, D.Q. Zhang, L.D. Wang, Y. Qiu, Chem. Commun. 47 (2011) 6467.
[63] H.J. Bolink, L. Cappelli, S. Cheylan, E. Coronado, R.D. Costa, N. Lardiés, M.K. Nazeeruddin, E. Ortí, J. Mater. Chem. 17 (2007) 5032.
[64] W.Y. Wong, G.J. Zhou, X.M. Yu, H.S. Kwok, Z.Y. Lin, Adv. Funct. Mater. 17 (2007) 315.